

Switching capability of double-sided grating with horizontal shift

Hideo Iizuka,^{1,a)} Nader Engheta,² Hisayoshi Fujikawa,³ Kazuo Sato,³ and Yasuhiko Takeda³

¹Toyota Research Institute, Toyota Motor Engineering and Manufacturing North America, Ann Arbor, Michigan 48105, USA

²Department of Electrical and Systems Engineering, University of Pennsylvania, Philadelphia, Pennsylvania 19104, USA

³Toyota Central Research and Development Laboratories, Nagakute, Aichi 480 1192, Japan

(Received 6 June 2010; accepted 18 July 2010; published online 4 August 2010)

A TiO₂ grating beam splitter on the SiO₂ layer is designed using the modal analysis. Normal incident light couples to the -1st/+1st-order transmission diffraction with a 49.6% efficiency for each and with a 50° refraction angle that is larger than the critical angle for the SiO₂-air interface. The SiO₂ interlayer is sandwiched between the two gratings. The finite-integration-technique investigation shows its switching capability due to the quarter-period shift between the gratings, with the zeroth-order transmission smaller than 5% for the “off” state and larger than 95% for the “on” state from 553 to 654 nm wavelength regime. © 2010 American Institute of Physics. [doi:10.1063/1.3476349]

Dielectric surface-relief gratings are among the key devices in optics and photonics. Resonant gratings with near 100% reflection filters^{1,2} have been designed for transmission filters,^{3,4} cavity resonators,⁵ and couplers for normal incident light to guided light.^{6,7} Tunability of reflection spectrum of resonant gratings has been studied for displays,⁸ where asymmetrical structure with the horizontal movement of grating ridges allows such tunability. A tunable transmission filter with the horizontal movement of the top and bottom gratings of identical shape has also been presented in Ref. 9. The two-grating structure in Ref. 9, however, has a gap of one-hundredth of wavelength in a Fabry–Perot cavity. The near field coupling modulation in Ref. 9 provided the wavelength shift in a resonant peak. Furthermore, it has been shown that the grating light valves with vertical movement of alternative metal ridges have led to tunability in reflection.¹⁰ In terms of the oblique diffraction orders, gratings have also been designed for solar cells,^{11,12} where the normal incident light is mainly coupled to the -1st/+1st and -2nd/+2nd-order transmission diffraction.¹² It is generally challenging to efficiently couple to only the -1st/+1st-order diffraction.

In this paper, a grating beam splitter with a refraction angle larger than the critical angle of the SiO₂-air interface is designed by exploiting the higher permittivity of the grating such as TiO₂ for the excited waveguide modes in the grating. When an SiO₂ interlayer is sandwiched between the two identical gratings, the structure provides the possibility of light switching between the top and the bottom gratings by applying a horizontal shift between the two gratings. The double-sided grating presented here utilizes the peak/zero electric field distribution engineered by the single grating, which is different from the mechanism of the structure in Ref. 9.

Figure 1(a) shows the configuration of the TiO₂ grating beam splitter attached on top of a semi-infinite SiO₂ layer. Two propagating ($m=0$ and 1) and other evanescent

($m \geq 2$) waveguide modes are excited along the z axis in the grating when the normally incident s -polarized light is illuminated upon the TiO₂ grating. The grating is designed as a beam splitter by coupling the incident wave mainly into the -1st/+1st-order transmission diffraction ($n=-1$ and $+1$) with the suppression of the zeroth-order diffraction ($n=0$). Selecting the grating period of $p=540$ nm, the -1st/+1st refraction angle is set at 50° at the design wavelength of $\lambda_0=600$ nm. This angle is larger than the critical angle of 43.6°

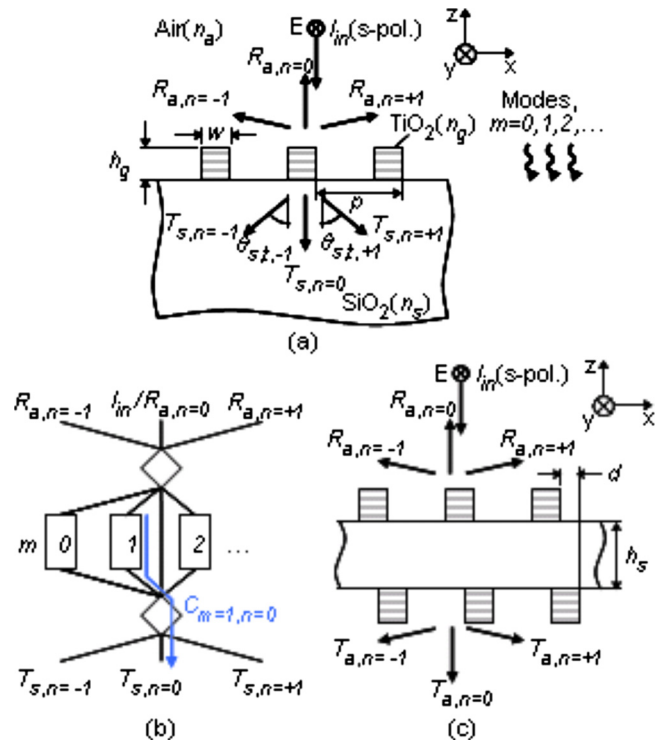


FIG. 1. (Color online) (a) Configuration and (b) equivalent circuit of the grating “beam splitter.” (dimensions; $p=540$ nm, $w=145$ nm, and $h_g=175$ nm, refractive index; $n_a=1$, $n_s=1.45$, and $n_g=2.38$, and -1st/+1st refraction angle; $\theta_{s,t,-1}=\theta_{s,t,+1}=50^\circ$ at $\lambda_0=600$ nm) (c) Configuration of double-sided grating with the switching capability [interlayer thickness; $h_s=260$ nm, and grating dimensions; same as 1(a)].

^{a)}Electronic mail: hideo.iizuka@tema.toyota.com.

for the SiO₂-air interface. The SiO₂ layer supports the zeroth and $-1\text{st}/+1\text{st}$ propagating ($n=-1, 0, +1$), and other evanescent ($n \geq 2$) diffraction orders in the operating wavelength range of 500 to 700 nm, while the air region has the zeroth and $-1\text{st}/+1\text{st}$ propagating diffraction orders ($n=-1, 0, +1$) from 500 to 540 nm, and only the zeroth propagating diffraction order ($n=0$) from 540 to 700 nm. The grating refractive index, $n_g=2.38$, and the ridge width, $w=145$ nm, are selected to excite two propagating waveguide modes ($m=0$ and 1) with equal amplitudes in the grating. The grating height, $h_g=175$ nm, corresponding to the propagation length of the waveguide mode, is chosen such that these two waveguide modes are out-of-phase at the grating's end. These result in the suppression of the zeroth-order transmission diffraction ($n=0$). Figure 1(b) shows the equivalent circuit for such waveguide modes. The coupling coefficient $C_{m,n}$ from the m th waveguide mode ($m=0, 1, \dots$) assigned from the largest eigenvalue) to the n th-order transmission diffraction ($n=-1, 0, +1$) is introduced by

$$T_{s,n} = \sum_m C_{m,n} \exp\{-jk_0[n_s^2 - (n\lambda_0/p)^2]^{1/2}h_g\} \\ \times \sum_m (1/p) \int_0^p X_m(x) \exp[-jk_0(n\lambda_0/p)x] dx [A_m \\ \times \exp(-j\Lambda_m h_g) + B_m \exp(j\Lambda_m h_g)], \quad (1)$$

where k_0 is the wave number in free space, A_m and B_m are amplitudes of the m th waveguide mode for the $+z$ and $-z$ directions, and Λ_m and $X_m(x)$ are the m th eigenvalue and eigenfunction in dispersion equation in the modal analysis given in Ref. 13. The double-sided grating consists of the SiO₂ interlayer sandwiched between the two identical gratings as shown in Fig. 1(c). The top and bottom gratings may be shifted horizontally by the distance, d .

In the Littrow mounting condition with oblique incidence, two propagating waveguide modes have the same amplitude even when the grating and the layer have the same permittivity, and the relative phase difference at the grating's end allows the -1st -order diffraction enhancement or $-1\text{st}/+1\text{st}$ -order splitting by the appropriate grating height.^{14–16} In the normal incidence case, the refractive index of the grating, n_g , has an important role to play in the functionality of this grating as a beam splitter. Figure 2(a) shows diffraction efficiency as a function of n_g at 600 nm. 11 waveguide modes were included in the calculation. The grating height, h_g , and the ridge width, w , were adjusted to maximize the $-1\text{st}/+1\text{st}$ -order diffraction at each n_g . As n_g is increased, the $-1\text{st}/+1\text{st}$ -order diffraction efficiency ($n=-1$ and $+1$) is increased while the zeroth-order diffraction efficiency ($n=0$) is decreased. Diffraction efficiency gives a $-1\text{st}/+1\text{st}$ -order transmission efficiency of 49.6% for each, with the zeroth-order suppressed to 0.5% at $n_g=2.38$. The results of the numerical investigation by the finite-integration-technique-based simulator, CST Microwave StudioTM,¹⁷ agree well with those by the modal analysis. This beam splitter characteristic of the TiO₂ grating can be understood in Fig. 2(b) for $C_{m,n}$. Not only is $m=0$ waveguide mode present but also $m=1$ waveguide mode is excited as n_g is increased. When the both waveguide modes are excited with equal amplitudes, the out-of-phase condition cancels out the zeroth-order transmission diffraction ($n=0$) as the appropriate grating height, h_g is used.

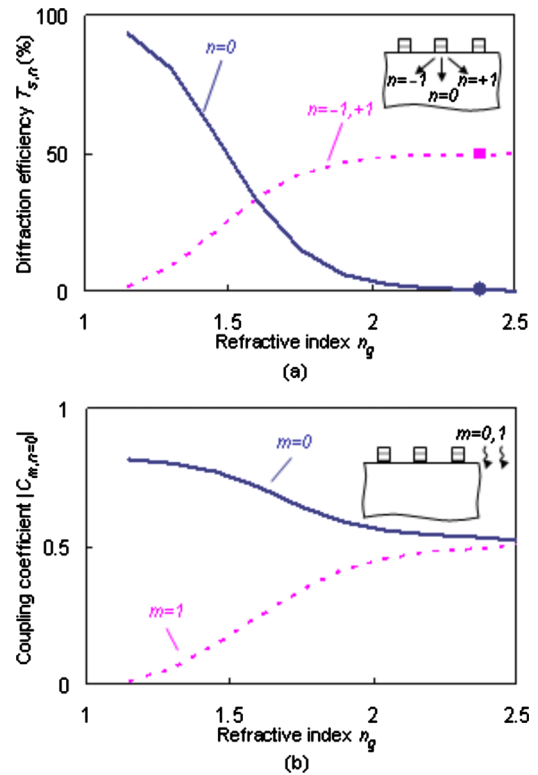


FIG. 2. (Color online) (a) Diffraction efficiency and (b) coupling coefficient of the grating beam splitter as a function of refractive index of grating at 600 nm operating wavelength. [Solid line and dashed line are obtained using the modal analysis. The single dots (shown as a “circle” and a “square”) are the results of the CST Microwave StudioTM simulation.]

Figures 3(a)–3(d) show the snapshot (in time) of the electric field distributions at 600 nm for four cases. In case of the semi-infinite SiO₂ layer in Fig. 1(a), each of the $-1\text{st}/+1\text{st}$ -order diffracted light propagates toward the $-50^\circ/+50^\circ$ direction in the SiO₂ layer (i.e., in-phase along the dashed line AA' for $+50^\circ$) due to the splitting of the incident light as shown in Fig. 3(a). There are alternating “plus” and “minus” peaks (i.e., standing wave) along the x direction (i.e., the dotted line BB'). As we see in this figure, the peaks

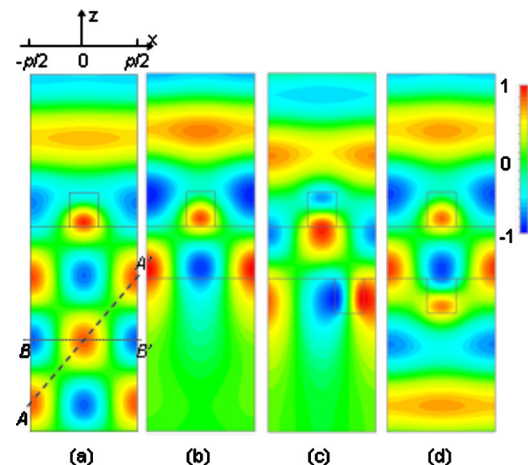


FIG. 3. (Color online) Snapshot (in time) of the electric field distributions at 600 nm operating wavelength. The electric field is normalized to the maximum value in each figure. (a) The SiO₂ layer with the top grating has the semi-infinite thickness. (b) The SiO₂ interlayer with the top grating has a finite thickness of $h_s=260$ nm. The top and bottom gratings have (c) the shift of a quarter period, and (d) no shift in the horizontal direction.

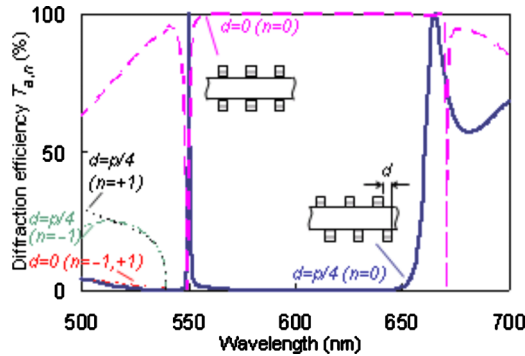


FIG. 4. (Color online) Diffraction efficiency of the transmission in the double-sided grating for the quarter-period shift and no shift.

of this standing wave in the SiO_2 layer happen at $x = -p/2, 0,$ and $+p/2$. This implies that nulls (i.e., the zero) of electric field are at $x = -p/4$ and $+p/4$. This peak/zero electric field distribution is the key point in the light coupling/decoupling phenomena between the top and bottom gratings in our proposed structure. Incident light reflects back at the bottom of SiO_2 -air interface when the SiO_2 interlayer has a thickness of 260 nm, as shown in Fig. 3(b). The interesting feature is that the incident light reflects back even when the bottom grating is attached with the horizontal shift of $d = p/4$, as shown in Fig. 3(c). The top grating provides the electric field peaks at $x = -p/2, 0,$ and $+p/2$ that correspond to the zero electric field regions for the bottom grating when shifted by $d = p/4$, resulting in light decoupling. It is worth noting that this phenomenon happens only in the case of the grating acting as a beam splitter with a refraction angle larger than the critical angle of the SiO_2 -air interface. Figure 3(d) shows the case of no shift, where light goes through with the zeroth-order transmission, since both the top and bottom gratings have the electric field peaks at $x = -p/2, 0,$ and $+p/2$.

Figure 4 shows the characteristics of the switching capability of the double-sided grating structure. The transmittance of the zeroth-order diffraction ($n=0$) is less than 5% from 552 to 654 nm at the horizontal shift of $d = p/4$, while it is larger than 95% from 553 to 670 nm with no shift, i.e., $d = 0$. This results in switching capability in the wavelength range of 553 to 654 nm, exhibiting a relatively wide bandwidth (16.7%) due to off-resonance. The range of switching is bounded by the resonances at the shorter and longer wave-

lengths. Between 500 and 540 nm, the incident light couples to the $-1\text{st}/+1\text{st}$ -order diffraction rather than to the zeroth-order diffraction for $d = p/4$, while the $-1\text{st}/+1\text{st}$ -order diffraction is much smaller than the zeroth-order diffraction for $d = 0$.

In conclusion, a grating beam splitter with a refraction angle greater than the critical angle of the SiO_2 -air interface was designed by utilizing the higher permittivity of TiO_2 with the two excited waveguide modes coupling to the $-1\text{st}/+1\text{st}$ -order (and near-zero coupling to the zeroth-order) transmission diffraction. Switching capability for such double-sided grating structures was achieved with the horizontal quarter-period shift of one grating with respect to the other. This switching capability can be used in a variety of scenarios and applications, such as lasers, the light emitting diodes and the window shutter for sun light illumination control with unpolarized designs. Moreover, the decoupling phenomenon at both gratings may also provide a helpful method for improving the efficiency in detectors and solar cells collecting light at both sides.

- ¹R. Magnusson and S. S. Wang, *Appl. Phys. Lett.* **61**, 1022 (1992).
- ²D. L. Brundrett, E. N. Glytsis, and T. K. Gaylord, *Opt. Lett.* **23**, 700 (1998).
- ³R. Magnusson and S. S. Wang, *Appl. Opt.* **34**, 8106 (1995).
- ⁴Y. Ding and R. Magnusson, *Opt. Lett.* **29**, 1135 (2004).
- ⁵F. Brückner, D. Friedrich, T. Clausnitzer, O. Burmeister, M. Britzger, E. B. Kley, K. Danzmann, A. Tunnermann, and R. Schnabel, *Opt. Express* **17**, 163 (2009).
- ⁶S. Ura, S. Murata, Y. Awatsuji, and K. Kintaka, *Opt. Express* **16**, 12207 (2008).
- ⁷S. Siitonen, P. Laakkonen, J. Tervo, and M. Kuittinen, *Opt. Express* **15**, 2008 (2007).
- ⁸R. Magnusson and M. Shokooh-Saremi, *Opt. Express* **15**, 10903 (2007).
- ⁹W. Nakagawa and Y. Fainman, *IEEE J. Sel. Top. Quantum Electron.* **10**, 478 (2004).
- ¹⁰O. Solgaard, F. S. A. Sandejas, and D. M. Bloom, *Opt. Lett.* **17**, 688 (1992).
- ¹¹C. Eisele, C. E. Nebel, and M. Stutzman, *J. Appl. Phys.* **89**, 7722 (2001).
- ¹²S. H. Zaidi, J. M. Gee, and D. S. Ruby, *Proceedings of the 28th IEEE Photovoltaic Specialists Conference* (IEEE, New York, 2000), p. 395.
- ¹³P. Sheng, R. S. Stepleman, and P. N. Sanda, *Phys. Rev. B* **26**, 2907 (1982).
- ¹⁴T. Clausnitzer, T. Kampfe, E.-B. Kley, A. Tunnermann, U. Peschel, A. V. Tishchenko, and O. Parriaux, *Opt. Express* **13**, 10448 (2005).
- ¹⁵J. Feng, C. Zhou, J. Zheng, and B. Wang, *Opt. Commun.* **281**, 5298 (2008).
- ¹⁶H. Iizuka, N. Engheta, H. Fujikawa, and K. Sato, *Microwave Opt. Technol. Lett.* **52**, 1362 (2010).
- ¹⁷CST Microwave Studio, 2009, <http://www.cst.com>.